ADVANCED MATERIALS
www.advmat.de

Self-Propulsion by Directed Explosive Emulsification

*Xuefei Wu, Han Xue, Gautam Bordia, Zachary Fink, Paul Y. Kim, Robert Streubel, Jiale Han, Brett A. Helms, Paul D. Ashby, Ahmad K. Omar, and Thomas P. Russell**

An active droplet system, programmed to repeatedly move autonomously at a specific velocity in a well-defined direction, is demonstrated. Coulombic energy is stored in oversaturated interfacial assemblies of charged nanoparticle-surfactants by an applied DC electric field and can be released on demand. Spontaneous emulsification is suppressed by an increase in the stiffness of the oversaturated assemblies. Rapidly removing the field releases the stored energy in an explosive event that propels the droplet, where thousands of charged microdroplets are ballistically ejected from the surface of the parent droplet. The ejection is made directional by a symmetry breaking of the interfacial assembly, and the combined interaction force of the microdroplet plume on one side of the droplet propels the droplet distances tens of times its size, making the droplet active. The propulsion is autonomous, repeatable, and agnostic to the chemical composition of the nanoparticles. The symmetry-breaking in the nanoparticle assembly controls the microdroplet velocity and direction of propulsion. This mechanism of droplet propulsion will advance soft micro-robotics, establishes a new type of active matter, and introduces new vehicles for compartmentalized delivery.

1. Introduction

A liquid–liquid interface, the narrow boundary separating two immiscible liquids, can be locked into a specific shape, that is, structuring the liquids, to tailor transduction pathways for the transport of charges, ions, particulates, or fluids within a fluid medium.[1–3] Transport within a fluid environment can also be achieved by moving droplets within the medium. But, developing strategies to make the propulsion of fluid droplets autonomous, repeatable, and directional remains a challenge.[4–9] Indeed, the experimental realization of self-propulsion or "activity" is an area of intense current research. Achieving directed motion necessarily requires the flow of energy into the system to break time-reversal symmetry. The form of this energy can be chemical, as in the case of self-propulsion resulting from diffusiophoresis or chemotaxis.[10] Alternatively, this energy can be provided through an external field, as with electrophoresis or phototaxis.[11,12] For liquid droplets, owing to lack of an inherit anisotropy, self-propulsion is usually achieved through a surface gradient in the interfacial tension (IFT), typically realized by a solubilization, chemical reaction, or surface phase transformation.[13–17] Such propulsion, though, is limited to the system with a continuous injection of chemical/light energy or the need of specifically engineered or chemically reactive materials, and lacks control over reversibility and repeatability. Generating a new mode of self-propulsion for swimming droplets that can be used with a broader range of the materials and does not require the continuous injection of external energy remains an outstanding challenge in active liquid systems.

Here, we show that a DC electric field can be used to oversaturate the surface of a liquid droplet with charged nanoparticle-surfactants (NPSs), agnostic to the chemical composition of the nanoparticles (NPs). The charges on the NPSs, coupled with the increased thickness of the interfacial assembly, increases the stiffness of the interfacial assembly[18–22] suppressing a spontaneous emulsification anticipated for such densely packed interfaces.[23] The increased dipole–dipole interaction also helps to stabilize the oversaturated packing of the interface. A Coulombic potential energy is stored in the oversaturated NPS assembly that upon rapid removal of the field, is released in the form of a plume of hundreds of thousands of charged microdroplets that are explosively ejected from the droplet surface, an event termed explosive

X. Wu, H. Xue, G. Bordia, Z. Fink, P. Y. Kim, J. Han, B. A. Helms, A. K. Omar, T. P. Russell
Materials Sciences Division
Lawrence Berkeley National Laboratory
Berkeley, CA 94720, USA
E-mail: russell@mail.pse.umass.edu

G. Bordia, J. Han, A. K. Omar
Department of Materials Science and Engineering
University of California Berkeley
Berkeley, CA 94720, USA

The ORCID identification number(s) for the author(s) of this article can be found under https://doi.org/10.1002/adma.202310435

Z. Fink, T. P. Russell
Polymer Science and Engineering Department
University of Massachusetts
Amherst, MA 01003, USA

R. Streubel
Department of Physics and Astronomy
University of Nebraska-Lincoln
Lincoln, NE 68588, USA

B. A. Helms, P. D. Ashby
Molecular Foundry
Lawrence Berkeley National Laboratory
Berkeley, CA 94720, USA

DOI: 10.1002/adma.202310435

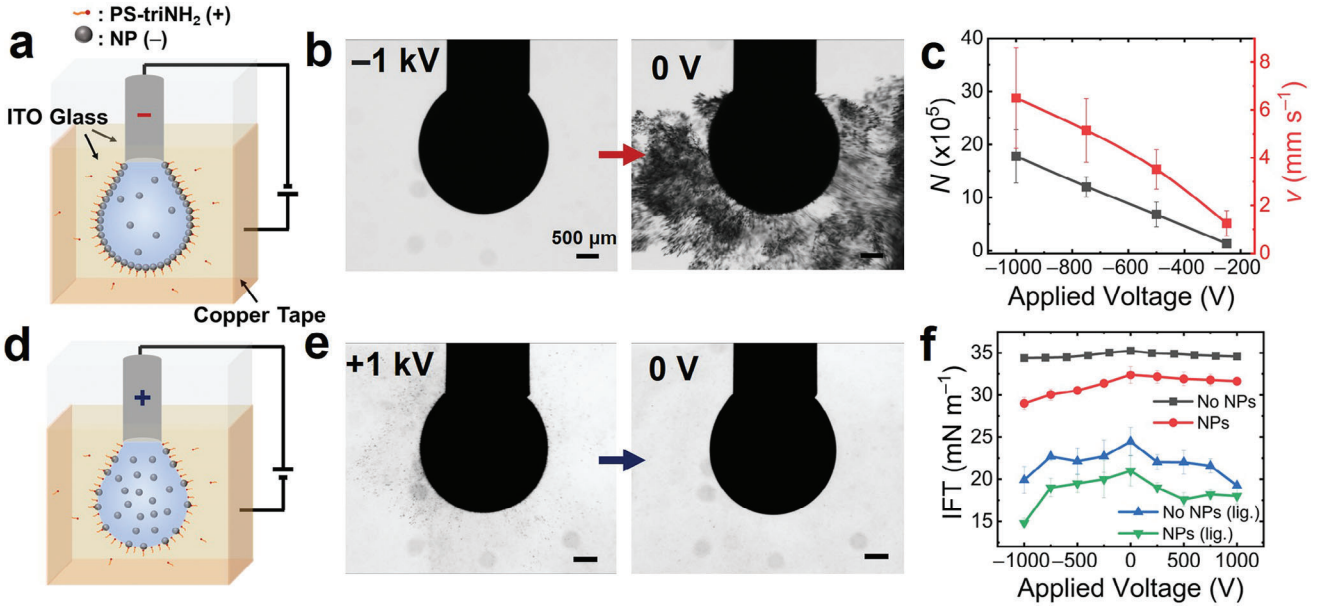

Figure 1. Schematic of the experimental setup. a,d) A pendant aqueous droplet is immersed in the toluene phase and hung at the end of a stainless-steel needle enabling application of a negative (a)/positive (d) bias voltage. The conductive chamber holding the polystyrene solution acts as the counter electrode; b) Optical images of the aqueous droplet (C_{Fe3O4} = 1 mg mL^{-1}) immersed in a PS-triNH$_2$ solution (1 mg mL^{-1}) in toluene under a bias voltage of −1000 V applied to the needle, and after the field is turned off; c) Total number, *N*, and mean velocity, *v*, of the jettisoned microdroplets generated during the explosive emulsification after different negative applied voltages are removed; e) Optical images of the aqueous droplet under the bias voltage of +1000 V applied to the needle, and after the field is turned off; f) Equilibrium IFT of a bare water/toluene (black squares), Fe_3O_4 NP dispersion (1 mg mL^{-1})/toluene (red circles), water/toluene solution of PS-triNH$_2$ (0.01 mg mL^{-1}) (blue triangles), and an aqueous dispersion of Fe_3O_4 NPs (1 mg mL^{-1})/toluene solution of PS-triNH$_2$ (0.01 mg mL^{-1}) (green triangles) under different applied voltages, where no spontaneous emulsification or explosive emulsification is observed. Scale bar: 500 μm.

emulsification. This event, accompanied with a sharp increase in the IFT, is two orders of magnitude more intense than that achievable by other means, indicating that the underlying mechanism is electrostatic in origin.[24] The explosive emulsification described here is distinct from prior research that used magnetic or electric fields to demulsify the emulsions[25] or tune their macroscopic properties by adjusting the emulsions interaction and microscale physical phenomena,[26–28] and also different from conventional rapid emulsification processes, for example, spontaneous emulsification[29] and electric emulsification.[23] For spontaneous emulsification, various mechanisms have been reported, for example, ultralow/negative interfacial tension[29–31] and supersaturation of surfactants/cosolvents at the interface.[32–36] The velocity at which microdroplets are ejected during spontaneous emulsification is significantly slower compared to that in explosive emulsions, and this process continues spontaneously until the system reaches equilibrium. In electric emulsification, rapid emulsification occurs only under high voltage, facilitated by the use of strong electric fields. These fields increase Coulombic repulsion at the interface, overcoming IFT and leading to the generation and ejection of droplets from the surface. This process ceases immediately when the high voltage is turned off, showing behavior that is distinctly different from explosive emulsification, which can quench the out-of-equilibrium self-assemblies at the interface by applying the external fields, allowing for controlled release of the stored energy. Furthermore, explosive emulsification holds promise for propulsion provided the ejected plume of charged microdroplets can be directed. This is accomplished by placing the droplet between two parallel electrodes, where an applied DC electric field breaks the symmetry of the interfacial assembly making the explosive emulsification highly directional. The repulsive force between the charged parent droplet and the plume of ejected charged microdroplets propels a millimeter-sized parent droplet centimeters in seconds. The droplet velocity can be tuned by the strength of the applied field. This self-propulsion does not require the constant injection of a chemical fuel and the propulsion, while triggered by the field, occurs only after the field is removed. The propulsion is repeatable and the direction of propulsion is controllable, making it of use in soft micro-robotics, compartmentalized micro-delivery systems, and smart materials. The propelled droplets can also be used as a model active matter system that may deepen our understanding of these out-of-equilibrium materials.

2. Results and Discussions

2.1. Field-Direction Dependence of Explosive Emulsification

Initial experiments were performed using a 1 mg mL^{-1} dispersion of 30 nm diameter carboxylic acid functionalized iron oxide NPs (Fe_3O_4-COOH NP) in water at a pH of 7.5. Droplets of these dispersions were suspended from a stainless-steel needle connected to an external power supply in a 1 mg mL^{-1} toluene solution of polystyrene-triamine (PS-triNH$_2$) (**Figure 1**). The negatively charged NPs interact with the protonated PS-triNH$_2$ at the interface forming NPSs that assemble at and irreversibly bind

to the interface, decreasing the IFT to an equilibrium value of 12 mN m^{-1} (see Figure S1, Supporting Information). In addition to minimizing the interfacial energy, the NPSs significantly enhance both the binding energy of individual NP[37] and the bending modulus of the interface,[38] thereby capable of stabilizing the oversaturated packing assemblies and effectively preventing the electric emulsification, even when subjected to high voltage. A voltage was applied across the needle to the conductive walls of the container holding the PS-triNH_2 solution making the field lines nearly normal to the surface of the droplet. The sign of the applied voltage led to dramatically different behavior. With the needle as the cathode (Video S1, Supporting Information), the droplet is stable until the voltage is turned off, then a plume of hundreds of thousands of microdroplets are ballistically jettisoned from the droplet surface (Figure 1a,b). The number and speed of the jettisoned microdroplets increases with the applied voltage (Figure 1c), and the total released energy is on the order of hundreds of nJ (Figure S2, Supporting Information), where the majority of the jettisoned microdroplets are spherical with an average diameter of 3.0 ± 1.2 µm. Cylindrical microdroplets, with typical lengths of 18.5 ± 9.8 µm and diameter of ≈1.5 µm, are also seen (Figure S3, Supporting Information), demonstrating that NPS assemblies on the microdroplet surfaces are jammed, preventing them from relaxing to a spherical shape.[1,2] Reversing the field direction (Video S2, Supporting Information) makes the droplet interface unstable, leading to a continuous field-induced emulsification, also known as electric emulsification,[23,39] that ceases when the voltage is turned off (Figure 1d,e). It should be noted that intensity of the explosive emulsification is dependent on the pH of the aqueous phase,[24] which affects the Columbic interactions between the NPSs and their interfacial activity. Under neutral pH conditions, there is a combination of both strong electrostatic repulsion and high interfacial packing density, capable of accumulating substantial potential energy at the interface and resulting in pronounced explosive emulsification.

The IFT for a pure water droplet suspended in toluene is 35 mN m^{-1}, independent of field strength for sufficiently small applied fields (black dots in Figure 1f).[40] A droplet of Fe_3O_4-COOH NPs in toluene reveals a slightly decreased IFT of 33 mN m^{-1} due to the limited segregation of negatively charged NPs to the inherently negatively charged water–toluene interface.[41] Applying a negative potential drop across the interface, drives the NPs with a high surface charge density (≈800 electrons per particle) to the liquid–liquid interface,[42,43] decreasing the IFT. A positive potential drop at the interface draws the NPs to the needle and depletes the interface of excess NPs while retaining the IFT at approximately the same level (red dots in Figure 1f). PS-triNH_2 acts as a surfactant and absent an applied field the IFT decreases to 25 mN m^{-1} at a concentration of 0.01 mg mL^{-1}. An applied field enhances the transport of uncharged PS-triNH_2 to the interface due to electrohydrodynamic flows generated on both sides of the interface,[44] causing the IFT to decrease more rapidly at high applied voltages (see Figure S4, Supporting Information). Although PS-triNH_2 is uncharged in toluene, the amine groups ($pKa_1 \approx 10$, $pKa_2 \approx 7.5$, and $pKa_3 \approx 4$) are protonated at neutral pH when it reaches the interface. This minimizes the interfacial energy and causes the field strength at which electric emulsification occurs to drop at high ligand concentration (Videos S3 and S4, Supporting Information).[23,39,45] The formation of NPSs further decreases the IFT to 21 mN m^{-1} when no field is applied (green dots in Figure 1f). Under a negative bias, the PS-triNH_3^+ forms NPSs with the excess NPs driven to the interface, overpacking the interface with NPSs and lowering the IFT to 15 mN m^{-1}. However, under a positive bias, the IFT decreases slightly at first, then remains virtually constant with increasing field strength, approaching the value without NPs, due to the depletion of the NPs from the interface.

2.2. Oversaturation of the NPSs at the Interface

Fluorescently labeled SiO_2 NPs functionalized with carboxylic acid groups show a similar behavior under an applied electric field (Figures S5 and S6, Supporting Information), providing a means to probe NPSs behavior in situ. Laser scanning fluorescence confocal microscopy images of fluorescently labeled, carboxy-functionalized SiO_2 NPs aqueous droplet suspended in a toluene solution of PS-triNH_2 show the accumulation of the NPSs at the droplet interface (**Figure 2**). A positive bias applied to the needle holding the droplet brightens the interface initially, but then it dims while the droplet interior increases in brightness, as the field pulls NPs (that have not formed NPSs) away from the interface into the droplet interior (Figure 2a). There is an increase in the concentration of PS-triNH_2 at the interface, as evidenced by the reduction in the IFT. The reduced IFT, combined with the in-plane electrostatic pressure, amplifies the interfacial fluctuations, inducing an electric emulsification, where spikes are seen to form at the interface. This electric emulsification removes NPSs from the surface of the parent drop causing the observed dimming (Video S5, Supporting Information). When the field is removed, the excess PS-triNH_2 and charge dissipate from the surface of the droplet, resulting in the increased IFT. This is followed by a gradual decrease in the IFT, as NPSs subsequently form and assemble at the interface (Figure S7, Supporting Information). The microdroplets located near the parent droplet surface are rapidly repelled from the droplet when the field is turned off, due to the like polarities of the microdroplets and droplet. No additional microdroplets form during this process (Video S2, Supporting Information).

A negative bias drives the negatively charged NPs to the interface where they interact with PS-triNH_3^+, forming stable NPSs, increasing the effective stiffness of the interface that suppresses field-induced emulsification. The number of NPSs at the interface increases, oversaturating the interface, as evidenced by the brighter fluorescence intensity (Figure 2a), and an enhancement in the fluctuations at the interface is seen. The densification of the NPSs under negative bias is also evident in in situ X-ray scattering measurements (Figure S8c, Supporting Information), clearly showing an excess of NPs being driven to and adsorbing onto the interface. Equally important, the X-ray scattering studies show that the assemblies remain liquid-like with no development of ordering. Under a positive bias, no such densification is observed. The results of the in situ X-ray scattering measurements are treated in full in a forthcoming manuscript.[46] We note, though, that these experiments were not performed on a pendant drop due to the absorption of the X-rays, but at the interface between an oil–water bilayer. Attempts were made to replicate the conditions of the pendant drop studies. The increased

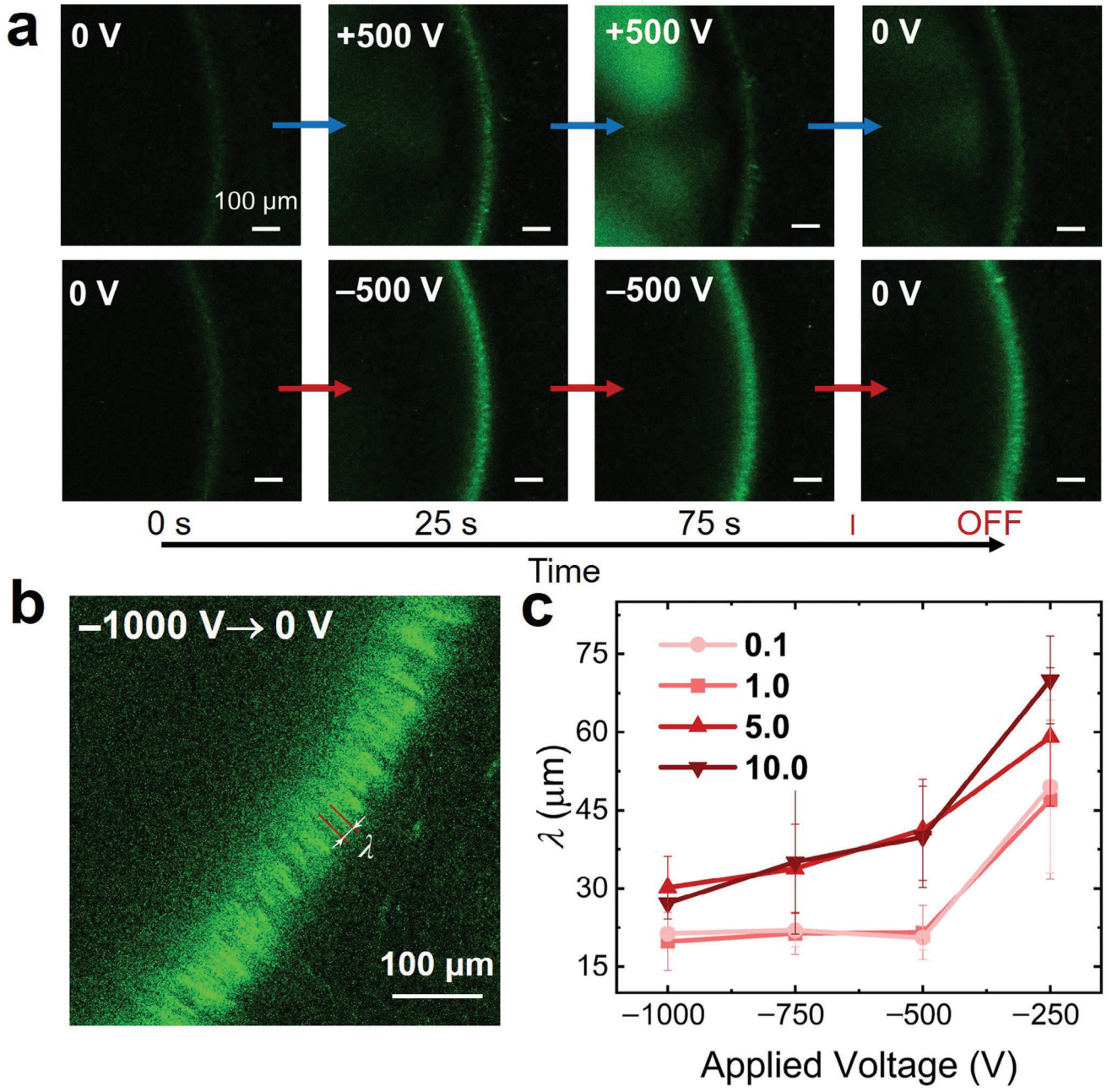

Figure 2. Microscope imaging of the NPSs under different applied voltages. a) Top row: a time-series of confocal images of the SiO_2 NPs aqueous droplet in toluene phase before, during, and after applying positive bias voltages, +500 V; bottom row: a time-series of confocal images of the same droplets before, during, and after applying −500 V. C_{SiO2} = 1 mg mL^{-1}, $C_{PS\text{-}triNH2}$ = 1 mg mL^{-1}; b) Confocal image of the water/oil interface right after switching off the voltage (−1000 V); c) Wavelength (λ) of the spikes formed after different negative voltages are turned off. The concentration of the SiO_2 varies from 0.1–10 mg mL^{-1} and the ligand concentration is 1 mg mL^{-1}.

dipole–dipole interaction also helps to stabilize the oversaturated packing structure at the interface. However, upon removal of the field, the chemical potential of the NPSs at the interface changes, as do interparticle interactions. Dipole interactions between the NPSs are absent,[47–49] causing an increased in-plane interfacial pressure and lowering of the IFT (**Figure** 3a and Video S6, Supporting Information). Fluctuations at the interface are further amplified, leading to thin fingers that extend from the interface, rapidly budding off microdroplets that are ballistically ejected, as the system returns to its original state absent a field (Figure 2b and Videos S7 and S8, Supporting Information).

A characteristic wavelength, λ, of the large-amplitude fluctuations emerges that decreases from ≈47 to ≈20 μm as the applied negative voltage increases from 250 to 10^3 V (Figure 2c and Figure S8, Supporting Information) and as the intensity of the explosive emulsification increases. The applied field across the

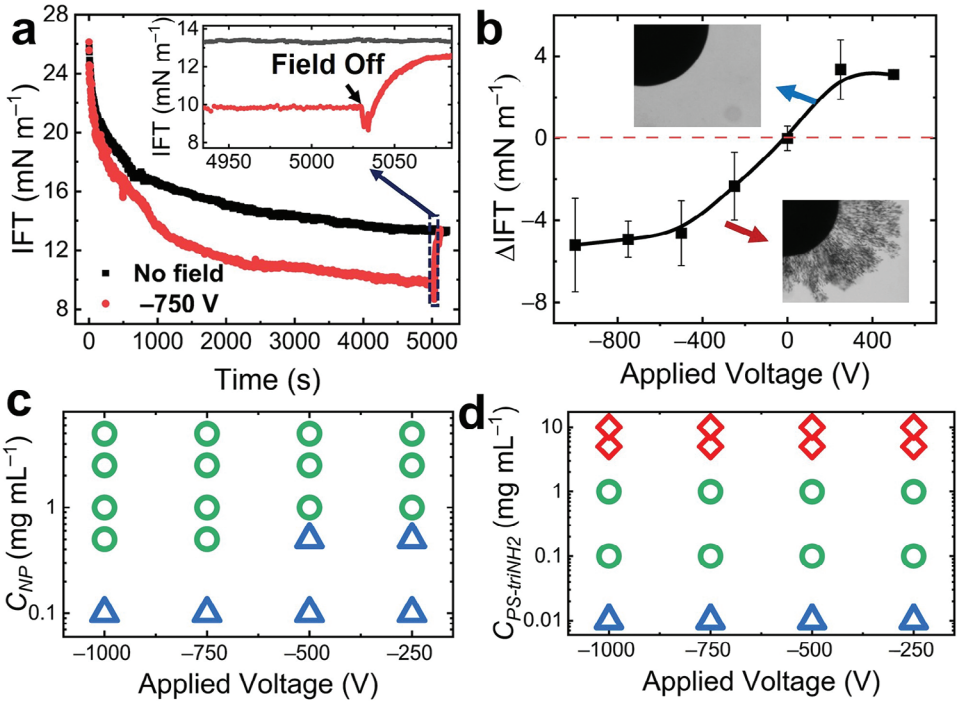

Figure 3. Electric field-driven oversaturation of NPSs at interface. a) Time evolution of the IFT under different applied voltages, 0 V (black) and −750 V (red), and the field is turned off at 5029 s. Inset is a magnified view of IFT plot within the designated rectangular area; b) Difference between the equilibrium IFT under 0 V and the minimum/maximum IFT after the field is switched off. The insets are the optical images of the droplet after the negative/positive bias voltage is turned off. c,d) The concentration of Fe_3O_4 and PS-triNH$_2$ are both 1 mg mL^{-1}; C_{Fe3O4} (c) and $C_{PS\text{-}triNH2}$ (d) dependencies of stable interface (blue triangle), explosive emulsification (green circle), and spontaneous emulsification (red diamond) behavior for various PS-triNH$_2$ and Fe_3O_4 concentrations. The $C_{PS\text{-}triNH2}$ is 0.1 mg mL^{-1} in (c) and C_{Fe3O4} is 1 mg mL^{-1} in (d).

interface produces an electrostatic pressure that amplifies fluctuations and, as the IFT decreases, λ decreases (Figure 3b).[50,51] However, by increasing the NP concentration to 5 and 10 mg mL^{-1}, λ increases to ≈70 µm due to the increase of effective stiffness of the interface at high NP concentrations (Figure S9, Supporting Information).[52,53]

The low areal density of NPSs formed at a fixed PS-triNH$_2$ concentration of 0.1 mg mL^{-1} and with [Fe_3O_4-COOH NP] ≤ 0.1 mg mL^{-1} suppresses an explosive emulsification at any of the applied voltages. For [Fe_3O_4-COOH NP] = 0.5 mg mL^{-1}, the achievable areal density increases, and explosive emulsification occurs for $V_{App} < -500$ V. Higher concentrations yield an explosive emulsification for $V_{App} \leq -250$ V (Figure 3c). In contrast, [Fe_3O_4-COOH NP] = 1 mg mL^{-1} and [PS-triNH$_2$] ≤ 0.01 mg mL^{-1} prevent explosive emulsification and [PS-triNH$_2$] ≥ 5 mg mL^{-1} triggers spontaneous emulsification (Figure 3d and Figure S10, Supporting Information) even without NPs and under no field.[54,55]

By adding salt the ionic strength of the aqueous phase is increased, charges are screened, and electrostatic repulsion between the NPSs on the interface are reduced allowing the areal density of the NPSs to increase and the IFT to decrease.[56,57] Consequently, electric emulsification is suppressed with a positive bias voltage, but, with a negative bias, explosive emulsification still occurs upon removal of the field, though at a significantly reduced ejection velocity (Figure S11, Supporting Information). We note that reducing the IFT typically promotes emulsification. However, the presence of salt screens the electrostatic interactions that are responsible for the explosive event, inhibiting electric emulsification and weakening the explosive emulsification.

2.3. Self-Propelled Droplets: Asymmetric Explosive Emulsification

In a uniform parallel electric field (**Figure 4a**), the droplet is polarized and the negatively charged NPs migrate to the side of the droplet closer to the positive electrode, promoting NPS formation on that side of the droplet (Figure S12; Videos S9 and S10, Supporting Information). Explosive emulsification is found to occur on that side of the droplet with ejected microdroplet velocities up to tens of mm s^{-1}. Upon ejection of the microdroplets the parent droplet is propelled in the opposite direction (Figure 4a). Similarly, if a plug of an aqueous NP dispersion is confined to a capillary tube (tilted at 3.3° from the horizontal) with PS-triNH$_2$ solutions on either side, the interface on the right moves ≈15 µm toward the negative electrode (Figure 4b), while an explosive emulsification pushes an entrapped air bubble downward, away from the interface. The interface on the left shows no observable displacement (Figure S13, Supporting Information).

Figure 5a shows an aqueous droplet (≈0.5 mm diameter) with dispersed NPs suspended in a toluene solution of PS-triNH$_2$

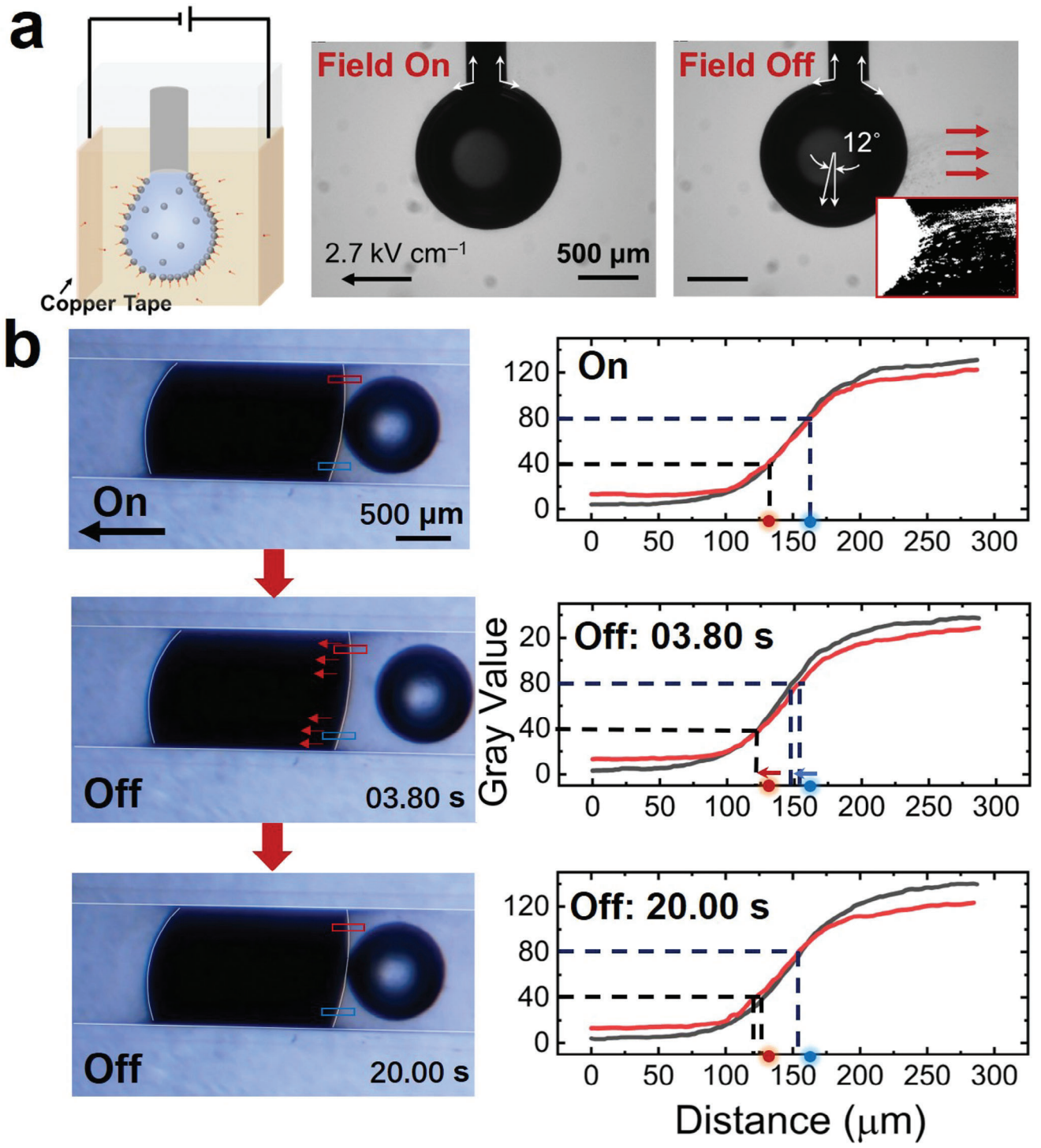

Figure 4. Asymmetric explosive emulsification. a) Left: Schematic of the experimental setup. A pendant aqueous droplet is immersed in the toluene phase and hung at the end of a stainless-steel needle. Two electrodes made of copper tape are attached to opposite walls of the container, enabling application of a uniform electric field across the droplet. Middle and right: aqueous droplet (C_{Fe3O4} = 1 mg mL^{-1}) immersed in the toluene phase ($C_{PS\text{-}triNH2}$ = 1 mg mL^{-1}) in the presence of a parallel electric field (2.7 kV cm^{-1}) and after turning it off. Inset shows binary contrast processed with ImageJ to highlight the droplet and microdroplets; b) The displacement of the interface caused by explosive emulsification. Aqueous phase (C_{Fe3O4} = 1 mg mL^{-1}) in a glass capillary tube (tilted at 3.3° from the horizontal) and with a toluene phase on either side ($C_{PS\text{-}triNH2}$ = 1 mg mL^{-1}); an air bubble is located at the right of the interface spontaneously due to the buoyancy. The optical microscopy images of the capillary tube, captured before and after the uniform electric field (3 kV cm^{-1}) turned off, are displayed in the left column. The gray value profile across the interface (red and blue boxes) as a function of horizontal distance is shown in the right column. The time values inserted in the images represent the duration that has passed after the electric field was turned off.

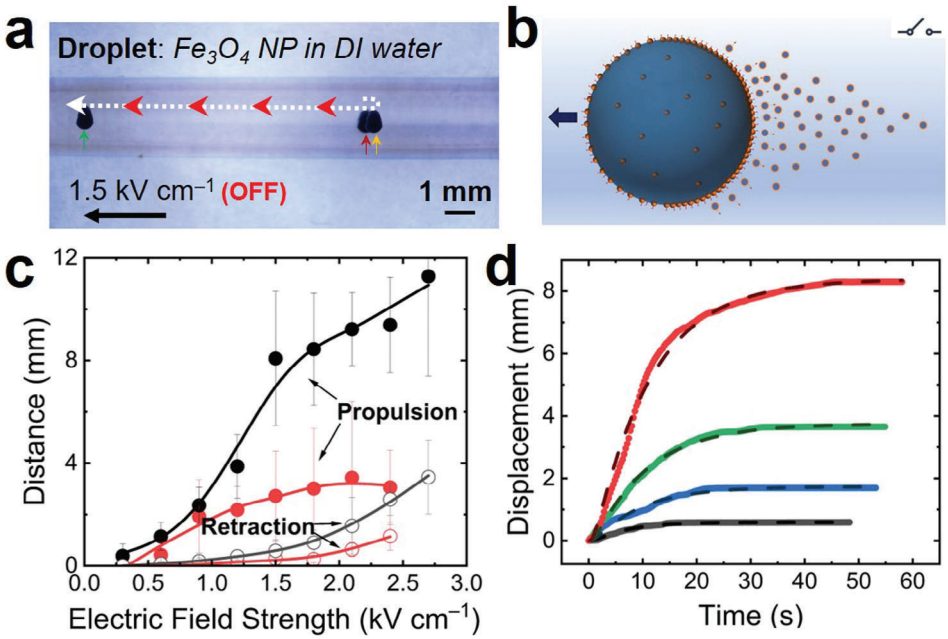

Figure 5. Self-propulsion movement. a) The dashed line with arrows indicates the trajectory of an aqueous droplet (C_{Fe3O4} = 1 mg mL^{-1}, ≈0.5 mm diameter) in the toluene phase ($C_{PS\text{-}triNH2}$ = 1 mg mL^{-1}) after a parallel electric field (1.5 kV cm^{-1}) is turned off, where the red, yellow, and green arrows mark the location of the aqueous droplet immediately after the field is turned off, when the retraction movement ceases, and when the self-propulsion movement comes to a halt, respectively; b) Schematics of the asymmetric packing of the NPSs at the surface of aqueous droplet that undergoes explosive emulsification at that side after the field turned off; c) Propulsion (solid circle) and retraction (empty circle) distance of the aqueous droplet (red circle: DI water; black circle: C_{Fe3O4} = 1 mg mL^{-1}) suspended in a toluene solution of PS-triNH$_2$ (1 mg mL^{-1}) within a polypropylene capillary tube after different parallel electric fields are turned off; d) Experimental displacement curves (solid lines) fit using Equation S17 (Supporting Information) (dashed lines) (see Appendix, Supporting Information) where τ and N_{tot} are fitting parameters and τ_B is set to 1 s. The four different field strengths used to induce explosive emulsification are 1.5 (red), 1.2 (green), 0.9 (blue), and 0.6 (black) kV cm^{-1}.

within a polypropylene capillary tube that is subjected to a parallel electric field along the axis of the capillary. When the field is removed, both the droplets with and without the NPs initially move toward the positive electrode, then stop, and reverse direction (Videos S11 and S12, Supporting Information). The initial retraction distance of the droplet without NPs is small and can be attributed to an electric emulsification arising from the accumulation of ligands on the negative electrode side. Removing the field causes the ligands to spread uniformly across the droplet surface, generating a Marangoni flow that moves the droplet toward the negative electrode.[13] However, the droplet, oversaturated with NPSs on the side near the positive electrode, begins to redistribute some NPSs to the depleted side of the droplet, causing the droplet to move initially toward the positive electrode (Marangoni flow). Then, explosive emulsification occurs rapidly ejecting a plume of charged microdroplets with velocities of 2.5 mm s^{-1} (1.5 kV cm^{-1}). Electrostatic repulsion between the plume of charged microdroplets and the parent droplet propels the charged parent droplet (surface charge density of ≈50 electrons μm^{-2}) over 8 mm, approximately ten times its size, toward the negative electrode (Figure 5b). The propulsion distance monotonically increases with the field strength (Figure 5c).

The propulsion velocity and subsequent displacement can be reproduced with a simple model, as detailed in the Supporting Information (Appendix, Supporting Information). The microdroplet dynamics are overdamped, a consequence of their small size and the viscosity of toluene. In the overdamped limit, we can infer the forces acting on the microdroplets by measuring their velocities and, using Newton's third law, estimate the (electrostatic) forces that the microdroplets exert on the parent droplet. It is precisely these forces that drive the parent droplet propulsion. The magnitude and duration of the active force dictate the displacement curve and are directly related to the number of microdroplets ejected, the rate of ejection, the degree of ejection asymmetry, and the microdroplet speed, all of which are governed by the field strength and geometry (see Appendix, Supporting Information). This model captures the experimental findings remarkably well, as shown in Figure 5d.

Similar behavior was also observed when an ≈3 μL droplet of an aqueous dispersion of NPs placed at the interface between solutions of PS-triNH$_2$ in CCl_4 (bottom layer) and toluene (top layer). Two electrodes with a separation distance of 35 mm were used to apply a field parallel to the interface between the fluids. A top view of the droplet trajectory is shown in **Figure 6a**. The droplet rapidly moves toward the negative electrode, triggering an electric emulsification on the droplet surface facing the negative electrode (Figure S14 and Video S13, Supporting Information). The emulsification decreases the excess charge on the droplet and the Coulombic forces acting on the droplet balance, and the velocity of the droplet steadily decreases until it comes to rest. Upon removing the field (bright blue line), the droplet velocity abruptly increases to ≈8 mm s^{-1}, where an explosive emulsification occurs on the negatively charged side of the droplet propelling the droplet in the opposite direction. Even with

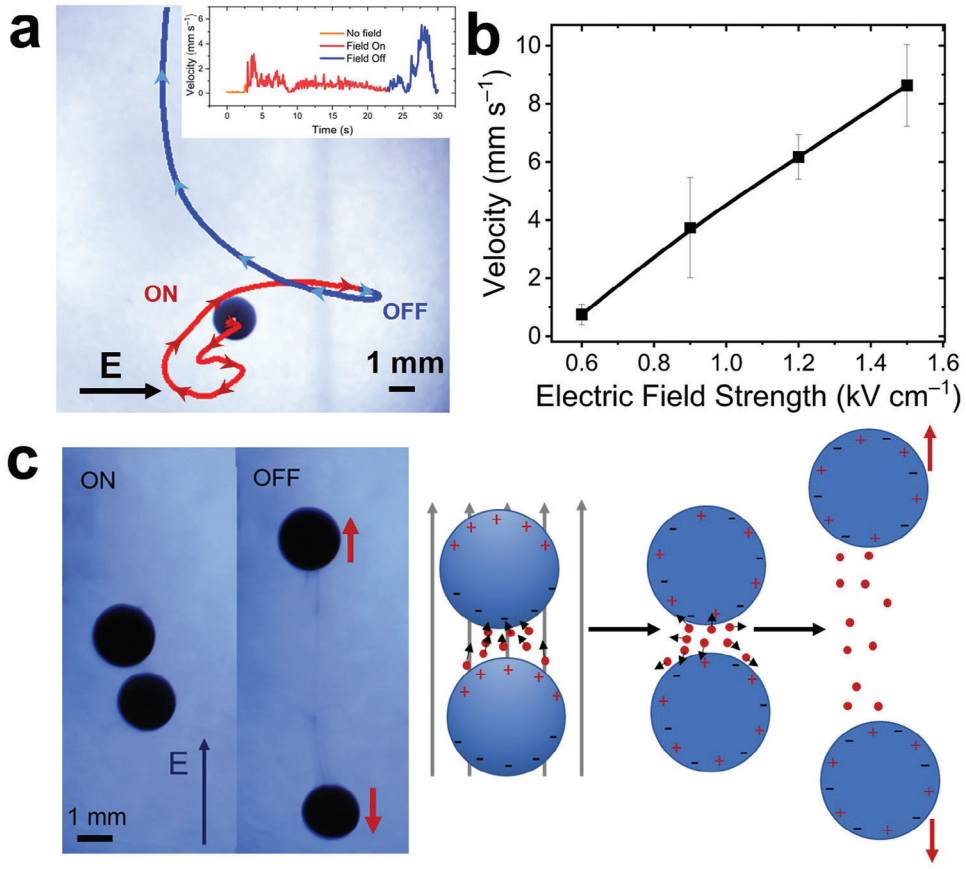

Figure 6. Self-propulsion movement of the droplet located at the toluene/CCl_4 interface. a) Trajectory of a 3 µL aqueous droplet (C_{Fe3O4} = 1 mg mL^{-1}) suspended at the interface between toluene and CCl_4 ($C_{PS\text{-}triNH2}$ = 1 mg mL^{-1} in both oil phase) before (orange), during (bright red), and after (bright blue) applying a parallel electric field of 1.2 kV cm^{-1}. The inset plot is the time evolution of the velocity of the aqueous droplet; b) The maximum propulsion velocity of the droplet varies with the parallel electric field strengths; c) Two aqueous droplets close to each other in the presence of a parallel electric field (1.2 kV cm^{-1}), and repel each other once the field is switched off. The concentration of PS-triNH$_2$ is 1 mg mL^{-1} and the concentration of Fe_3O_4 is 1 mg mL^{-1}. Scale bar: 1 mm.

a larger ≈10 µL droplet, explosive emulsification efficiently propels the droplet (Video S14, Supporting Information). The force generated for propulsion increases with increasing field strength and so does the droplet velocity (Figure 6b and Figure S15, Supporting Information). It should be noted that the multi-curved trajectory of the self-propelled droplets at the toluene/CCl_4 interface mainly stems from the density gradient of the surrounding medium and the asymmetric overpacking of the NPSs. These factors lead to a deviation from the perfect spherical shape of the droplets. Moreover, the confined space within the container introduces a boundary effect, further influencing the movement of the droplets and resulting in a multi-curve trajectory. If we introduce a second droplet to the interface, when the field is applied and the droplets polarized, the droplets can be strongly attracted to each other, inducing an electro-coalescence. This attraction, if strong enough, can cause the formation of a liquid bridge between the droplets, a redistribution of the charges on the droplet surfaces, causing an electrostatic repulsion.[58,59] Here the result shows electric emulsification occurring in the gap between the droplets. As the field is turned off, the charges on the surfaces of the droplets redistribute and the droplets repel each other (Figure 6c).

3. Conclusion

We have demonstrated an advanced form of active matter that can be programmed to repeatedly move at a specific velocity in a well-defined direction. A DC electric field is used to oversaturate the surface of a liquid droplet with charged NPSs, agnostic of chemical composition of the NPs, storing a Coulombic energy. On demand the field is released causing the formation of hundreds of thousands of charged microdroplets that are electrostatically repelled from the droplet in an explosive emulsification event. The explosive emulsification is made directional by breaking the symmetry of the interfacial assembly, propelling the droplet large distances in the opposite direction. The propulsion is autonomous and repeatable and the direction can be changed with each cycle. This propulsion can be leveraged for microactuation in soft micro-robotics compartmentalized micro-delivery systems, and smart materials. Since the explosive emulsification behavior is independent of the chemical nature of the NPs, the explosive emulsification can be harnessed to serve as a unique delivery mechanism for spray-coating surfaces of objects in situ, controlling chemical reaction, or enhancing delivery of water-soluble materials in organic environment.

4. Experimental Section

Sample Preparation: The negatively charged carboxylic acid-functionalized iron oxide NPs (Fe_3O_4-COOH) (Ocean NanoTech) and green fluorescently labeled silica NPs (SiO_2-COOH) (Micromod) with diameters of ≈30 nm were dispersed in deionized water and suspended in a solution of ω-(diethylene triamine)-terminated polystyrene (PS-triNH_2, M_w = 1200 g mol^{-1}) (Polymer Source) in toluene/CCl_4 (Sigma-Aldrich). Carboxylic acid functionalized gold NPs (Au NPs) were prepared by the Turkevich methods, and with diameter of ≈12.2 nm. Fe_3O_4/SiO_2 NPSs were formed by the interaction of the NPs with the PS-triNH_2 at the interface of the immiscible liquids. All nanoparticle dispersions were used without further purification and diluted to the required concentration using deionized water.

Titration Experiment: To determine the amount of carboxyl groups on each Fe_3O_4-COOH NP, the back titration experiment was conducted (Figure S16, Supporting Information). The Fe_3O_4 NPs with carboxylic acid groups used in these experiments were purchased from Ocean Nanotech. Poly(maleic anhydride-alt-1-octadecene) was used to modify the surface of these NPs. Subsequent hydrolysis of this compound leads to the formation of carboxyl groups, enhancing the stability of the NPs in aqueous solutions. The Fe_3O_4-COOH NPs were first to react with an excess amount of NaOH (1 M). After complete reaction, the residual NaOH, mol_{OH-} were measured by titration with HCl solution (pH 3.4), and the consumption of the HCl was denoted as "n_0." Upon adding the acid solution, an increasing number of deprotonated carboxyl groups reacted with protons, and two pKa values were observed. These values arise from the two neighboring carboxyl groups. After one of the two carboxyl groups had completely reacted, the total consumption of HCl was denoted as "n_1." Thus, the number of carboxyl groups on individual NP (N_{COOH}) could be calculated with the following equation

$$N_{COOH} = \frac{2\,(n_1 - n_0)\,N_A}{N_{Fe3O4}} \quad (1)$$

where N_A is Avogadro's number, and N_{Fe3O4} is the number of the Fe_3O_4-COOH NP used in the titration which could be identified by their mass concentration. To minimize the effect of CO_2 from the air, the open end of the vial was covered with parafilm during titration.

Electric Field Experiment: Axisymmetric electric fields were applied to the pendant droplet suspended from stainless-steel needle (15 Gauge) by connecting the latter to a high-voltage generator (Trek 615-10). The voltage supply was grounded to the outer surface of cuvette (12.5 mm × 12.5 mm × 45 mm), which was covered on two opposite sides and the bottom with conductive copper tape and the remaining two opposite walls were ITO glass for clear view. A constant bias voltage was applied to the needle without any current. The microdroplets in the electric field experiments were imaged using an Olympus DSX1000 microscope. To apply a parallel electric field on the suspended droplet, two opposite sides of the cuvette were covered by a copper tape, connected to the bias voltage, and grounded separately.

IFT Measurement: A pendant drop tensiometer (Krüss DSA30) was used to measure the IFT. The time dependence of IFT was recorded after the aqueous droplet (≈30 µL) was injected into the oil phase until the IFT reached equilibrium. An axisymmetric electric field was applied to the pendant droplet during the measurement to investigate the influence of applied voltage on IFT.

Confocal Measurement: A Zeiss LSM710 confocal microscope was used to investigate the behavior of the NPSs under an electric field microscopically. A homemade sample cell was designed to put on top of the objective (10×), and a pendant aqueous droplet surrounded by the toluene phase was placed in the cell. The axisymmetric/parallel electric fields were applied on the pendant drops during the measurement.

In Situ X-Ray Scattering Measurement: Scattering experiments were conducted at the advanced light source at Lawrence Berkeley National Laboratory, utilizing beamline 7.3.3 and employing 10 keV X-rays across a q range from 0.004 to 3.5 Å^{-1}. A water–oil interface was generated within a 5 mm quartz capillary tube with a wall thickness of 0.01 mm (Charles Supper). The interface establishment involved initially filling the capillary with the Au NP dispersion, followed by carefully layering a toluene solution of PS-triNH_2 atop the aqueous dispersion. Electrodes were positioned, with one beneath the capillary tube and another above the oil phase, to create a uniform electric field across the interface, with a 25 mm spacing between them. This configuration ensured a uniform electric field-oriented perpendicular to the interface. To precisely locate the vertical position of the interface, the beam was scanned from the oil phase to the aqueous phase, identifying the interface through a sharp decrease in transmitted intensity. Upon locating the interface, the sample underwent a 20-s exposure to the beam for scattering measurement on a Pilatus area detector. The notable discrepancy in electron density between Au and the toluene oil phase induced significant scattering from the NPSs assembled at the interface. Horizontal averaging of scattering profiles showed maxima at a characteristic q^* value, indicating the center-to-center distance between NPSs at the interface, $d = 2\pi/q^*$.

Propulsive Experiment Measurement: A 3.5 cm-wide square cuvette was used to observe the trajectory of a 3 µL droplet of an aqueous dispersion of the functionalized NPs placed at the interface between CCl_4 (bottom) and toluene (bottom) solutions of PS-triNH_2. Two parallel conductive plates on the sides of the cell were used to apply a parallel field on the droplet, and the strength of the uniformly applied parallel electric field, E, is calculated using the formula $E = \frac{V}{d}$, where V represents the bias voltage, and d denotes the separation distance between the electrodes, which in this case, also corresponds to the width of the square cuvette. Optical microscopy (AmScope) was used to record the movement of the droplet, and the trajectory of the droplet was analyzed using Matlab.

The mobility of the droplet was studied using a capillary tube. A droplet of an aqueous dispersion of NPs was place in a 1.5 mm diameter glass capillary tube forming a liquid plug in the capillary. Toluene solution of PS-triNH_2 was placed on both sides of the aqueous plug and an air droplet was place on one side of the plug using an inclination angle of 3.3° to force the air droplet to the water/oil interface. Electrodes at the ends of the capillary tube were used to apply a parallel electric field across the components. In a separate experiment, a droplet of an aqueous dispersion of the NPs was placed in a larger polypropylene capillary tube (2.4 mm diameter) in a toluene solution of PS-triNH_2. The diameter of the droplet was smaller than the inner diameter of the capillary to allow the droplet to freely move.

Analysis on the Explosive Emulsification: The jettisoned microdroplets during the explosive emulsification were identified and tracked with ImageMagick, an imaging processing tool. The optical images were converted into a black and white format, a process that is exemplified in Figure S17 (Supporting Information). For quantifying the microdroplets, the areas occupied by the needle and the parent droplet were first subtracted from the overall white area in the image. And the total number of the jettisoned microdroplets was then estimated by dividing the projection area of each individual microdroplet from the remaining white area. It should be noted that this estimation did not account for overlapping microdroplets due to the absence of 3D imaging capabilities in the current experimental setup, which makes the authors' estimate a lower bound. The velocities of the microdroplets were calculated using OpenPIV (Particle Image Velocimetry).

Supporting Information

Supporting Information is available from the Wiley Online Library or from the author.

Acknowledgements

X.W. and H.X. contributed equally to this work. This work was supported by the U.S. Department of Energy, the Office of Science, the Office of Basic Energy Sciences, the Materials Sciences and Engineering Division under Contract No. DE-AC02-05-CH11231 within the Adaptive Interfacial Assemblies Towards Structuring Liquids program (KCTR16). R.S. acknowledges

support by the National Science Foundation (NSF), the Division of Materials Research (DMR) under grant no. 2203933. Work at the Molecular Foundry was supported by the Office of Science, the Office of Basic Energy Sciences, of the U.S. Department of Energy under Contract No. DE-AC02-05CH11231. Beamline 7.3.3 of the Advanced Light Source is supported by the Director of the Office of Science, the Office of Basic Energy Sciences, of the U.S. Department of Energy under Contract No. DE-AC02-05CH11231.

Conflict of Interest

The authors declare no conflict of interest.

Data Availability Statement

The data that support the findings of this study are available in the supplementary material of this article.

Keywords

charged nanoparticle-surfactants, directed explosive emulsification, liquid–liquid interface, self-assembly, self-propulsion

Received: October 8, 2023
Revised: February 15, 2024
Published online:

[1] M. Cui, T. Emrick, T. P. Russell, *Science* **2013**, *25*, 460.
[2] J. Forth, P. Y. Kim, G. Xie, X. Liu, B. A. Helms, T. P. Russell, *Adv. Mater.* **2019**, *31*, 1806370.
[3] G. Xie, J. Forth, Y. Chai, P. D. Ashby, B. A. Helms, T. P. Russell, *Chem* **2019**, *5*, 2678.
[4] D. Cholakova, M. Lisicki, S. K. Smoukov, S. Tcholakova, E. E. Lin, J. Chen, G. De Canio, E. Lauga, N. Denkov, *Nat. Phys.* **2021**, *17*, 1050.
[5] S. T. Chang, V. N. Paunov, D. N. Petsev, O. D. Velev, *Nat. Mater.* **2007**, *6*, 235.
[6] J. R. Baylis, J. H. Yeon, M. H. Thomson, A. Kazerooni, X. Wang, A. E. S. John, E. B. Lim, D. Chien, A. Lee, J. Q. Zhang, J. M. Piret, L. S. Machan, T. F. Burke, N. J. White, C. J. Kastrup, *Sci. Adv.* **2015**, *1*, e1500379.
[7] J. G. Gibbs, Y.-P. Zhao, *Appl. Phys. Lett.* **2009**, *94*, 163104.
[8] Z. Zhan, F. Wei, J. Zheng, W. Yang, J. Luo, L. Yao, *Nanotechnol. Rev.* **2018**, *7*, 555.
[9] R. Dreyfus, J. Baudry, M. L. Roper, M. Fermigier, H. A. Stone, J. Bibette, *Nature* **2005**, *437*, 862.
[10] C. Jin, C. Kruger, C. C. Maass, *Proc. Natl. Acad. Sci. USA* **2017**, *114*, 5089.
[11] J. Tonga, D. Wanga, Y. Liua, X. Lou, J. Jiang, B. Dong, R. Dong, M. Yang, *Proc. Natl. Acad. Sci. USA* **2021**, *118*, 2104481118.
[12] C. Lozano, B. Ten Hagen, H. Lowen, C. Bechinger, *Nat. Commun.* **2016**, *7*, 12828.
[13] D. Babu, N. Katsonis, F. Lancia, R. Plamont, A. Ryabchun, *Nat. Rev. Chem.* **2022**, *6*, 377.
[14] C. Kurzthaler, L. Gentile, H. A. Stone, *Out-of-Equilibrium Soft Matter: Active Fluids*, Royal Society of Chemistry, London **2023**.
[15] T. Toyota, N. Maru, M. M. Hanczyc, T. Ikegami, T. Sugawara, *J. Am. Chem. Soc.* **2009**, *131*, 5012.
[16] C. C. Maass, C. Krüger, S. Herminghaus, C. Bahr, *Annu. Rev. Condens. Matter Phys.* **2016**, *7*, 171.
[17] P. Dwivedi, D. Pillai, R. Mangal, *Curr. Opin. Colloid Interface Sci.* **2022**, *61*, 101614.
[18] B. Loubet, P. L. Hansen, M. A. Lomholt, *Phys. Rev. E* **2013**, *88*, 062715.
[19] R. Bradbury, M. Nagao, *Soft Matter* **2016**, *12*, 9383.
[20] H. A. Faizi, S. L. Frey, J. Steinkuhler, R. Dimova, P. M. Vlahovska, *Soft Matter* **2019**, *15*, 6006.
[21] P. A. Barneveld, D. E. Hesselink, F. A. M. Leermakers, J. Lyklema, J. M. H. M. Scheutjens, *Langmuir* **1994**, *10*, 1084.
[22] P. A. Barneveld, J. M. H. M. Scheutjens, J. Lyklema, *Langmuir* **1992**, *8*, 3122.
[23] A. Watanabe, K. Higashitsuji, K. Nishizawa, in *Colloidal Dispersions and Micellar Behavior* (Ed: K. L. Mitta), American Chemical Society, Washington, DC **1975**, p. 97.
[24] X. Wu, G. Bordia, R. Streubel, J. Hasnain, C. C. S. Pedroso, B. E. Cohen, B. Rad, P. Ashby, A. K. Omar, P. L. Geissler, D. Wang, H. Xue, J. Wang, T. P. Russell, *Adv. Funct. Mater.* **2023**, *33*, 2213844.
[25] H. Yang, S. Wang, W. Zhang, J. Wu, S. Yang, D. Yu, X. Wu, Y. Sun, J. Wang, *Sci. Rep.* **2020**, *10*, 16565.
[26] S. S. Belykh, K. V. Erin, *Opt. Spectrosc.* **2021**, *129*, 1200.
[27] A. R. Zakinyan, L. M. Kulgina, A. A. Zakinyan, S. D. Turkin, *Fluids* **2020**, *5*, 74.
[28] S. S. Belykh, C. V. Yerin, *Bull. Russ. Acad. Sci.: Phys.* **2019**, *83*, 878.
[29] J. Hasnain, Y. Jiang, H. Hou, J. Yan, L. Athanasopoulou, J. Forth, P. D. Ashby, B. A. Helms, T. P. Russell, P. L. Geissler, *J. Chem. Phys.* **2020**, *153*, 224705.
[30] T. Okazawa, J. Bron, *J. Colloid Interface Sci.* **1979**, *69*, 86.
[31] L. M. Prince, *J. Colloid Interface Sci.* **1967**, *23*, 165.
[32] D. Cholakova, Z. Vinarov, S. Tcholakova, N. D. Denkov, *Curr. Opin. Colloid Interface Sci.* **2022**, *59*, 101576.
[33] G. J. Hirasaki, C. A. Miller, O. G. Raney, M. K. Poindexter, D. T. Nguyen, J. Hera, *Energy Fuels* **2010**, *25*, 555.
[34] K. J. Ruschak, C. A. Miller, *Ind. Eng. Chem. Fundam.* **1972**, *11*, 534.
[35] C. A. Miller, *Colloids Surf.* **1988**, *29*, 89.
[36] A. Bozeya, A. Al-Bawab, S. E. Friberg, C. A. Miller, *J. Dispers. Sci. Technol.* **2013**, *34*, 1429.
[37] S. Shi, T. P. Russell, *Adv. Mater.* **2018**, *30*, 1800714.
[38] J. Forth, A. Mariano, Y. Chai, A. Toor, J. Hasnain, Y. Jiang, W. Feng, X. Liu, P. L. Geissler, N. Menon, B. A. Helms, P. D. Ashby, T. P. Russell, *Nano Lett.* **2021**, *21*, 7116.
[39] B. Vonnegut, R. L. Neubauer, *J. Colloid Sci.* **1952**, *7*, 616.
[40] R. Sengupta, A. S. Khair, L. M. Walker, *J. Colloid. Interface Sci.* **2020**, *567*, 18.
[41] K. Roger, B. Cabane, *Angew. Chem., Int. Ed. Engl.* **2012**, *51*, 5625.
[42] M. E. Flatté, A. A. Kornyshev, M. Urbakh, *J. Phys.: Condens. Matter* **2008**, *20*, 073102.
[43] B. Su, J.-P. Abid, D. J. Fermin, H. H. Girault, H. Hoffmannova, P. Krtil, Z. Samec, *J. Am. Chem. Soc.* **2004**, *126*, 915.
[44] S. Mhatre, S. Simon, J. Sjoblom, *Anal. Chem.* **2020**, *92*, 12860.
[45] M. A. Nawab, S. G. Mason, *J. Colloid Sci.* **1958**, *13*, 179.
[46] X. Wu, H. Xue, Z. Fink, B. A. Helms, P. D. Ashby, A. K. Omar, T. P. Russell, unpublished.
[47] B. A. Grzybowski, K. Fitzner, J. Paczesny, S. Granick, *Chem. Soc. Rev.* **2017**, *46*, 5647.
[48] A. A. Harraq, B. D. Choudhury, B. Bharti, *Langmuir* **2022**, *38*, 3001.
[49] S. O. Lumsdon, E. W. Kaler, O. D. Velev, *Langmuir* **2004**, *20*, 2108.
[50] E. Schäffer, T. Thurn-Albrecht, T. P. Russell, U. Steiner, *Nature* **2000**, *403*, 874.
[51] Z. Lin, T. Kerle, S. M. Baker, D. A. Hoagland, E. Schäffer, U. Steiner, T. P. Russell, *J. Chem. Phys.* **2001**, *114*, 2377.
[52] A. Mikkelsen, Z. Rozynek, *ACS Appl. Mater. Interfaces* **2019**, *11*, 29396.
[53] J. Huang, M. Juszkiewicz, W. H. de Jeu, E. Cerda, T. Emrick, N. Menon, T. P. Russell, *Science* **2007**, *317*, 650.
[54] S. Aslan, A. Firoozabadi, *Langmuir* **2014**, *30*, 3658.
[55] S. B. de Araujo, M. Reyssat, C. Monteux, G. G. Fuller, *Sci. Adv.* **2019**, *5*, eaax8227.

[56] S. E. Anachkov, S. Tcholakova, D. T. Dimitrova, N. D. Denkov, N. Subrahmaniam, P. Bhunia, *Colloids Surf., A* **2015**, *466*, 18.
[57] Y. Chai, A. Lukito, Y. Jiang, P. D. Ashby, T. P. Russell, *Nano Lett.* **2017**, *17*, 6453.
[58] X. Luo, H. Yin, J. Ren, H. Yan, Y. Lü, L. He, *J. Phys. Chem. C* **2019**, *123*, 19588.
[59] W. D. Ristenpart, J. C. Bird, A. Belmonte, F. Dollar, H. A. Stone, *Nature* **2009**, *461*, 377.